

Combined Effects of Focused Ultrasound and Photodynamic Treatment for Malignant Brain Tumors Using C6 Glioma Rat Model

Junwon Park^{1*}, Chanhong Kong^{1*}, Jaewoo Shin¹, Ji Young Park¹, Young Cheol Na²,
Seung Hee Han³, Jin Woo Chang¹, Seung Hyun Song⁴, and Won Seok Chang¹

¹Department of Neurosurgery, Brain Research Institute, Yonsei University College of Medicine, Seoul, Korea;

²Department of Neurosurgery, Catholic Kwandong University College of Medicine, International St. Mary's Hospital, Incheon, Korea;

³Department of Medical Biophysics, University of Toronto, Toronto, Canada;

⁴Department of Electronics Engineering, Sookmyung Women's University, Seoul, Korea.

Purpose: Glioblastoma (GBM) is an intractable disease for which various treatments have been attempted, but with little effect. This study aimed to measure the effect of photodynamic therapy (PDT) and sonodynamic therapy (SDT), which are currently being used to treat brain tumors, as well as sono-photodynamic therapy (SPDT), which is the combination of these two.

Materials and Methods: Four groups of Sprague-Dawley rats were injected with C6 glioma cells in a cortical region and treated with PDT, SDT, and SPDT. Gd-MRI was monitored weekly and 18F-FDG-PET the day before and 1 week after the treatment. The acoustic power used during sonication was 5.5 W/cm² using a 0.5-MHz single-element transducer. The 633-nm laser was illuminated at 100 J/cm². Oxidative stress and apoptosis markers were evaluated 3 days after treatment using immunohistochemistry (IHC): 4-HNE, 8-OHdG, and Caspase-3.

Results: A decrease in tumor volume was observed in MRI imaging 12 days after the treatment in the PDT group ($p < 0.05$), but the SDT group showed a slight increase compared to the 5-Ala group. The high expression rates of reactive oxygen species-related factors, such as 8-OHdG ($p < 0.001$) and Caspase-3 ($p < 0.001$), were observed in the SPDT group compared to other groups in IHC.

Conclusion: Our findings show that light with sensitizers can inhibit GBM growth, but not ultrasound. Although SPDT did not show the combined effect in MRI, high oxidative stress was observed in IHC. Further studies are needed to investigate the safety parameters to apply ultrasound in GBM.

Key Words: Focused ultrasound, glioblastoma, treatment, sonodynamic therapy, photodynamic therapy, sono-photodynamic therapy

Received: September 15, 2022 **Revised:** February 9, 2023

Accepted: February 16, 2023 **Published online:** March 24, 2023

Co-corresponding authors: Seung Hyun Song, PhD, Department of Electronics Engineering, Sookmyung Women's University, 100 Cheongpa-ro 47-gil, Yongsan-gu, Seoul 04310, Korea.

E-mail: shsong.ee@sookmyung.ac.kr and

Won Seok Chang, MD, PhD, Department of Neurosurgery, Yonsei University College of Medicine, 50-1 Yonsei-ro, Seodaemun-gu, Seoul 03722, Korea.

E-mail: changws0716@yuhs.ac

*Junwon Park and Chanhong Kong contributed equally to this work.

•The authors have no potential conflicts of interest to disclose.

© Copyright: Yonsei University College of Medicine 2023

This is an Open Access article distributed under the terms of the Creative Commons Attribution Non-Commercial License (<https://creativecommons.org/licenses/by-nc/4.0>) which permits unrestricted non-commercial use, distribution, and reproduction in any medium, provided the original work is properly cited.

INTRODUCTION

Glioblastoma (GBM) is one of the most malignant tumors, and the life expectancy of patients with GBM is less than 15 months.¹ A concurrent chemo-radiation therapy using temozolomide followed by adjuvant chemotherapy is the standard therapy for GBM.^{2,3} However, due to its high recurrence rate, GBM is not completely curable,⁴ and relapse of the disease over a short period occurs in most patients due to the residual cancer cells.⁵ Therefore, other treatment modalities, such as photodynamic therapy (PDT), can be considered as an alternative option for recurrent GBM.⁶

PDT, which uses photosensitizers and light to treat tumors, is used for treating various cancers, such as advanced lung, skin,

and urinary cancers, since 1976.^{7,8} When the light at a specific wavelength is applied to the sensitizer, cytotoxic reactive oxygen species (ROS) are generated during energy absorption and released by the sensitizer, resulting in cell death.⁹ The sensitizer used in PDT accumulates at the tumor more specifically compared to normal tissue, which makes it a tumor-specific therapy.¹⁰ Several attempts were made to adapt these properties to apply PDT in brain tumors.¹¹

However, there are serious obstacles to applying PDT to brain tumors. When light is focused on the brain tissue, scattering of light inhibits it to transmit equally to all the fields and to reach the deep-seated tumor.¹² Therefore, technologies that can enhance light delivery into the brain are required for the application of PDT to GBM.¹³ Currently, many efforts are being made, such as increasing the number of light sources or developing bio-implantable light sources, to overcome this limitation.^{14,15} In addition, unlike other carcinomas, there are currently no standard guidelines for using PDT in GBM in clinical trials.

Changing the source of energy can be considered as another approach to resolving this problem. Among the various sources of energy, ultrasound used in the clinical field has been attempted.¹⁶ Activating sensitizer with low-intensity ultrasound is called sonodynamic therapy (SDT), and the therapeutic process and predictive mechanisms of SDT are similar to those of PDT.^{17,18} Reinforced by the development of focused ultrasound (FUS) sonication technique at intracranial tissue, SDT is drawing attention as a promising method to overcome energy permeation, the biggest drawback of PDT, and is being developed

steadily.^{16,19} Some studies have demonstrated the enhanced penetration of light by simultaneous application of ultrasound.^{20,21} In addition, sono-photodynamic therapy (SPDT), which combines PDT and SDT, is also gaining attention. SPDT increases therapeutic efficacy as two energies are applied simultaneously, but has mostly been demonstrated in vitro or in other organs, such as the liver.^{22,23} Thus, this study aimed to investigate the possibility of applying SPDT to treat GBM when compared with PDT and SDT (Fig. 1).

MATERIALS AND METHODS

All animal experimental procedures were approved by the Institutional Animal Care and Use Committee (2019-0005) of Yonsei University. Animals were housed in groups of three in laboratory cages with food and water available ad libitum under a 12-h light/dark (lights on at 07:00) cycle in a room with controlled temperature ($22\pm 2^\circ\text{C}$) and humidity ($55\pm 5\%$).

Tumor modeling with C6 cell and SD rat

C6 cells were obtained from ATCC (Cat. No. CCL-107). The cells were grown in F-12K (Kaighn's Modification of Ham's F-12) medium, supplemented with 2.5% heated fetal bovine serum and horse serum to a concentration of 15% at 37°C in 5% carbon dioxide at 90% relative humidity. The cells were thawed at a concentration of 5×10^5 in a 10-cm cell culture dish. After one subculture process, the cells were counted with trypan blue ex-

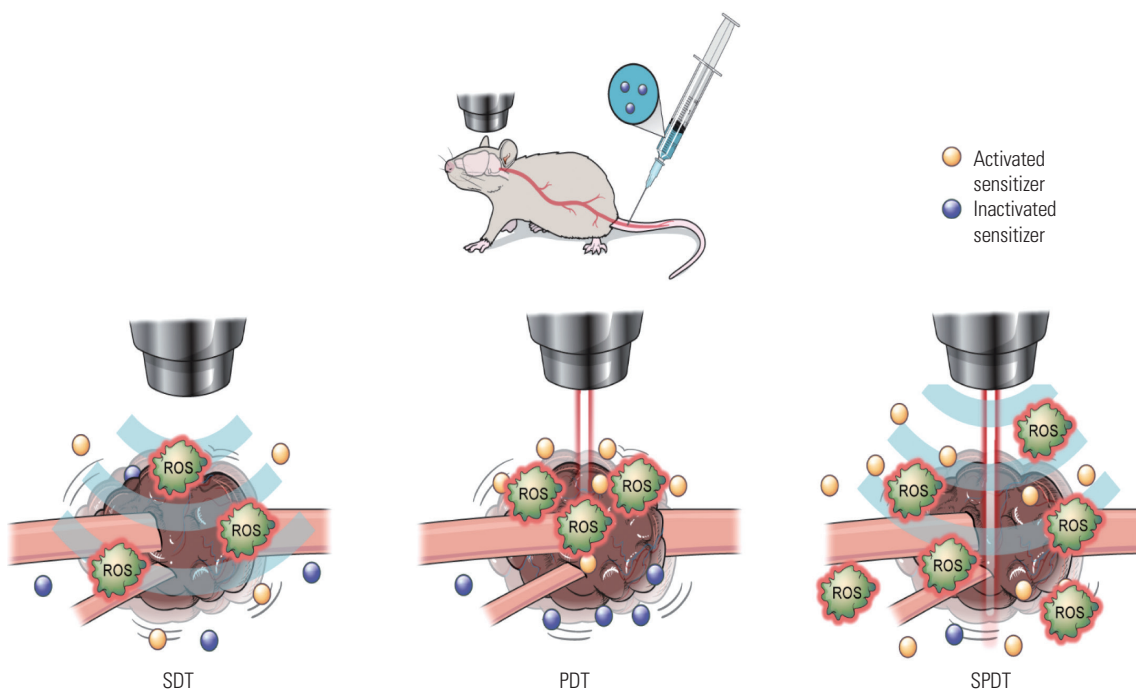


Fig. 1. Diagrammatic summary of each treatment. 5-ALA dissolved in saline was intravenously injected 6 h before treatment (60 mg/kg). SDT uses ultrasound as an energy source, which is permeable to tissue, and PDT uses light energy as a source to activate the sensitizer. For SPDT, both energies are simultaneously delivered to the tumor. SDT, sonodynamic therapy; PDT, photodynamic therapy; SPDT, sono-photodynamic therapy.

clusion and suspended in phosphate-buffered saline (PBS) according to their capacity.

Forty-two adult male Sprague-Dawley rats (weight: 250–270 g) were used. All animals were anesthetized with a mixture of ketamine (75 mg/kg), xylazine (Rompun, Elanco, Seoul, Korea; 4 mg/kg), and acepromazine (0.75 mg/kg), and fixed in a stereotaxic frame. A hole was made in the skull below the incised skin at the following points: from the bregma to the anterior-posterior, 0 mm; and medial-lateral 2 mm. Moreover, 1×10^5 of C6 cells suspended in PBS were slowly injected at a rate of 1 μ L/min using a syringe pump (Legato 130, 788130, KD Scientific, Holliston, MA, USA) to the following points: dorsal-ventral, -2.5 mm. The needle was kept for 5 min and removed slowly over another 3 min to prevent the backflow of the cells. The skin was sutured with 4-0 polydioxanone and removed after 2 weeks of treatment.

Sensitizer

The 5-aminolevulinic acid hydrochloride (5-ALA, Gliolan, Ver-to Korea, Seoul, Korea; 60 mg/kg) was used as the sensitizer. 5-ALA was applied to every rat used in this study. Right before injection, 5-ALA was dissolved in 0.9% sterile normal saline at 60 mg/mL and intravenously injected 6 h before each treatment at 60 mg/kg dose.

PDT

Prior to irradiation, the animals were anesthetized with a mixture of ketamine (75 mg/kg), xylazine (Rompun; 4 mg/kg), and acepromazine (0.75 mg/kg), and were fixed in a stereotaxic frame. Craniotomy was performed with a drill tip diameter of approximately 3 mm to apply energy of light effectively. A laser diode with a wavelength of 637 nm (LP637-SF70, Thorlabs Inc, Newton, NJ, USA) was used to generate continuous waves during the PDT. The output light from the end of the fiber, coupled with the laser diode, was collimated using a colli-

mator (F260FC-B, Thorlabs Inc). The turning on/off of the laser diode was controlled using a compact laser diode controller (CLD1010LP, Thorlabs Inc). When using this system and inputting 280 mV of power, 52 mW was measured with a power meter (PM100D, Thorlabs Inc). The laser was applied for 11 min 30 s with 52 mW of energy to obtain an area of 100 J/cm². Light energy was irradiated into the same position continuously during treatment using a custom-manufactured tool (Fig. 2A). After the treatment was completed, the condition of the animals was monitored during suturing, and no animal died after the treatment.

SDT

Anesthesia and craniotomy were performed similarly as in PDT before sonication. FUS energy was generated using a 0.5-MHz single-element spherically focused transducer (H-107MR, Sonic Concept Inc., Bothell, WA, USA) with a diameter of 51.7 mm and a radius of curvature of 63.2 mm. A waveform generator (33220A, Agilent, Palo Alto, CA, USA) was connected to a 50-dB radio frequency power amplifier (240 L, ENI Inc., Rochester, NY, USA) to drive the FUS transducer, and a power meter (E4419B, Agilent) was used to measure the input electrical power. The transducer was mounted on a cone filled with degassed water and the end of the tip was wrapped in a polyurethane membrane. For SDT, ultrasound energy was sonicated for 20 minutes to give a power density of 5.5 W/cm².²⁴ The process after the treatment was the same as that for PDT.

SPDT

All the pre-treatment procedures were the same for PDT. However, in SPDT, the two treatment methods were performed simultaneously. Both the laser diode and the waveform generator were operated simultaneously at the start of treatment (Fig. 2B). The laser diode was turned off after 11 min 30 secs; and the waveform generator was turned off after another 8 min 30 s to complete sonication. The post-treatment process was the

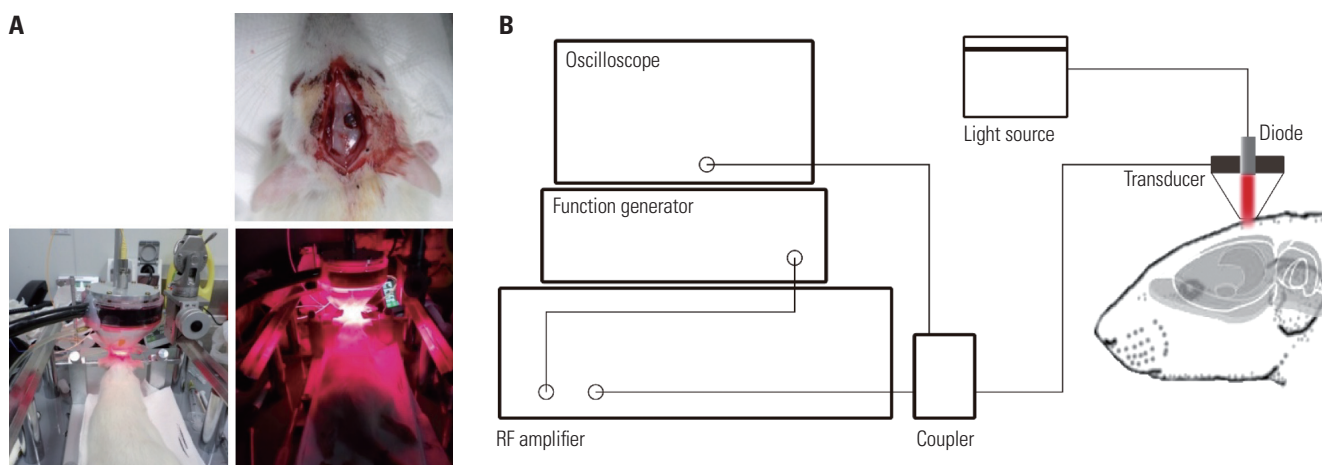


Fig. 2. Diagram of the treatment system. (A) The figure above shows the craniotomy before each treatment. (A) The figure below shows the power of the light generated in the laboratory when the light was turned off during the PDT treatment process. (B) Schematic diagram of the equipment. PDT, photodynamic therapy.

same as that for PDT.

MRI

MRI was performed 7 days after C6 cell implantation in rats three times a week with a Bruker 9.4 T 20-cm bore MRI system (Biospec 94/20 USR; Bruker, Ettlingen, Germany) and a rat head coil. Animals were anesthetized by 2% isoflurane inhalation during the MRI. A gadolinium-based MRI contrast agent, gadobutrol (Gadovist, Bayer, Leverkusen, Germany; 0.2 mL/kg), was injected intravenously, and contrast-enhanced T1-weighted images were used to confirm the tumor volume each week. The Elekta Gamma Plan software (Elekta, Stockholm, Sweden), used mainly in clinical practice, was used to calculate the tumor volume by setting the contrast-enhancement area as the region of interest (ROI) using the T1-weighted image (echo time; 2 ms, repetition time; 8.06 ms, echo train length; 2 ms, slice thickness; 1 mm). For statistical analysis, four animals were included in each study group.

18F-FDG-PET

The animals were anesthetized with 2% isoflurane inhalation during PET imaging. F-18 fluorodeoxyglucose (FDG) was intravenously injected into rats, and PET imaging was performed using a Siemens Inveon PET scanner (Siemens Medical Solutions USA Inc., Knoxville, TN, USA). Imaging was performed for 20 min, 1 h after intravenous FDG injection to confirm the change in tumor metabolism using glucose. The injected dose was 48.25 ± 1.95 MBq per rat. PET images were analyzed using the PMOD software (PMOD version 4.1, PMOD Technologies Ltd., Zurich, Switzerland).

Immunohistochemistry (IHC)

The brains were fixed with 4% paraformaldehyde for 24 h and embedded in paraffin. Sections were cut into 5- μ m coronal sections. The deparaffinization step and heat-mediated antigen retrieval were performed using 1X citrate buffer (boiling for 15 min at 85°C, cooling down for 30 min). Each section was washed in 1X PBS and incubated in blocking solution (1X PBS, 5% normal goat serum, 0.2% Triton X-100) for 2 h at room temperature. Sections were incubated with primary antibodies in blocking solution overnight at 4°C. The following primary antibodies were used: 4-HNE (4-Hydroxynonenal, Abcam, Cambridge, MA, USA; ab48506, 1:250), 8-OHdG (8-Hydroxy-2'-deoxyguanosine, Abcam, ab48508, 1:250), and Cas-3 (cleaved Caspase-3, Asp175, antibody#9661, 1:250). After the primary immunoreaction, the sections were incubated with Alexa 488 (Invitrogen, A11008, 1:500) and Alexa 594 (Abcam, A150156, 1:500) conjugated secondary antibodies for 2 h at room temperature. Nuclei were stained with DAPI (Thermo Fisher Scientific, Waltham, MA, USA; D1306, 1:1000) during conjugation with secondary antibodies. Immunostaining of the sections was visualized using an Axio Imager M2 (Carl Zeiss, Jena, Germany). Images were analyzed using the ImageJ software (Ver-

sion 1.52a, Bethesda, MD, USA), and the intensity of each fluorescence was calculated using the custom code of MATLAB software (Version 9.10, MathWorks, Boston, MA, USA).

Data analysis

Statistical analysis of IHC was performed using the extracted intensity values. For accurate image analysis, the ROI of the tumor was set based on DAPI. Then, four random places were selected in the tumor. Each factor's expression levels were compared after threshold value processing to remove artifacts, and intensity quantification was performed using MATLAB. The intensity values quantified after each treatment were compared with the group injected with only 5-ALA. All data are expressed as mean \pm standard error of the mean (SEM). The data were analyzed using one-way analysis of variance (ANOVA) followed by Uncorrected Fisher's LSD and the Kruskal-Wallis test. Statistical significance was set at $p < 0.05$. All statistical analyses were performed using the GraphPad Prism 7 software (GraphPad Software Inc., San Diego, CA, USA).

RESULTS

PDT and SPDT groups showed decreased volume in MRI

MRI was performed once weekly for 3 weeks to observe changes in tumor volume from 1 week after tumor implantation by using T1 contrast-enhanced imaging (Fig. 3A), and the results are shown in Fig. 3B. There was no significant difference in each group's tumor volume at 5 days after each treatment ($p = 0.46$ for Kruskal-Wallis test) (Fig. 3C). However, there was a difference at 12 days after the treatment (Fig. 3D). The tumor volume differed significantly between the group infused with 5-ALA alone (111.5 ± 31.81 mm³) and in the PDT group (20.5 ± 8.82 mm³; $p = 0.02$). In addition, there was a significant difference between SPDT (43.5 ± 19.14 mm³; $p = 0.002$) and PDT groups ($p < 0.001$) compared with the SDT group (174 ± 28.22 mm³). There was no significant difference between SPDT and PDT groups ($p = 0.5$). Interestingly, in the PDT group, the tumor volume decreased significantly from 5 days (58.25 ± 18.26 mm³) to 12 days after PDT ($p = 0.04$) (Fig. 3E). There was no significant change in the SPDT group from 5 days (53 ± 7.82 mm³) to 12 days after treatment, but a slight decrease was observed ($p = 0.73$) (Fig. 3F). This result shows that light energy had successfully activated the sensitizer in reduced tumor volume.

PDT and SPDT groups showed decreased glucose uptake in PET

One of the important characteristics of tumors is the activated uptake of glucose due to its high cell density and rapid growth. Therefore, 18F-FDG-PET was performed to observe treatment-induced changes in tumor activity. PET was also performed before and after each treatment, and two animals were ran-

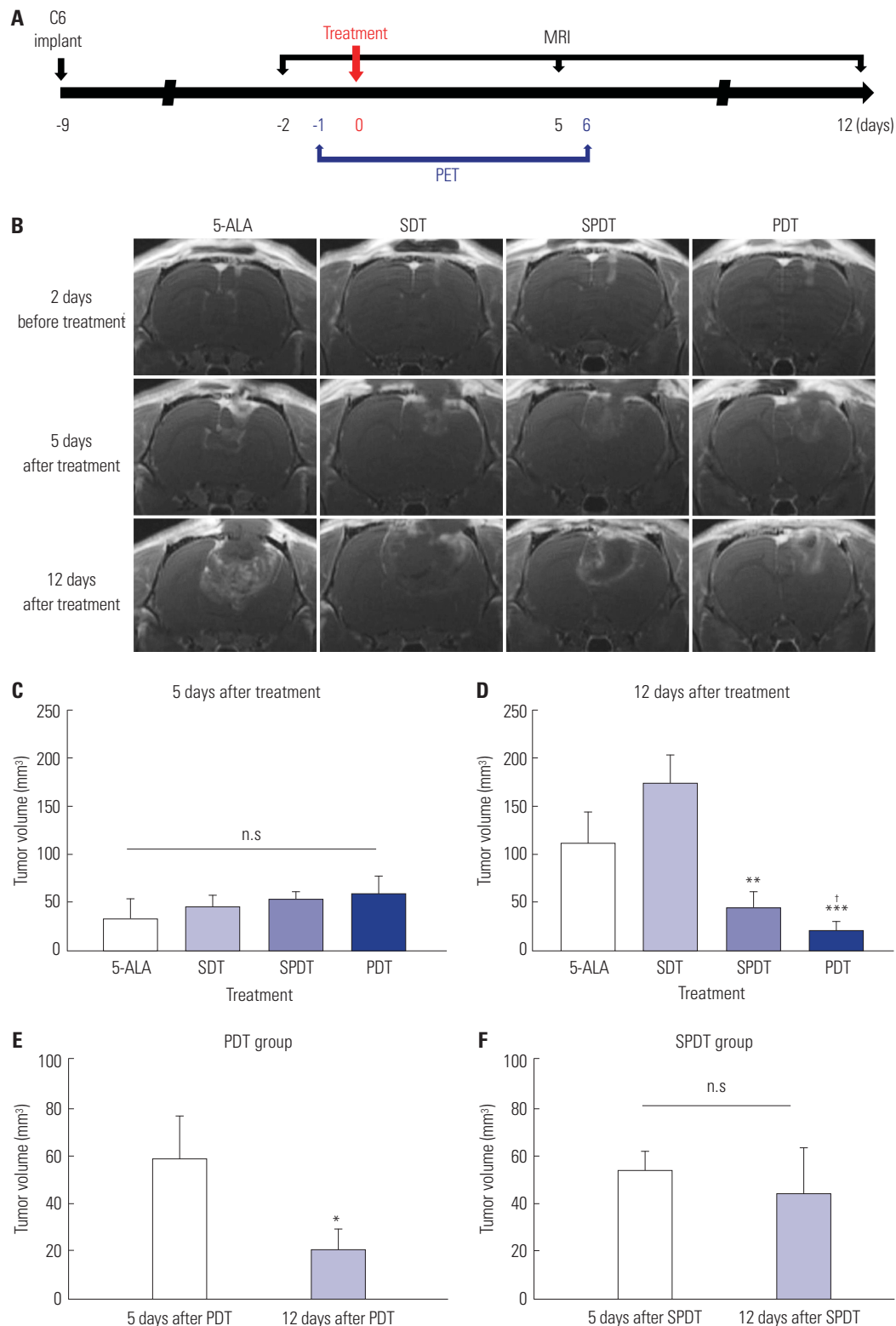


Fig. 3. Representative images of MRI and qualitative analysis of tumor volume with enhanced site MRI scan. Data are presented as means±SEM. (A) Timeline of MRI and PET for the analysis of tumor volume. (B) Representative T1-weighted MRI image by week in each group. (C) Bar graphs show the tumor volume 5 days after each treatment. Statistical analyses were performed using the Kruskal-Wallis test. There was no statistical significance between each group. (D) Bar graphs show the tumor volume 12 days after each treatment. Statistical analyses were performed using one-way analysis of variance followed by uncorrected Fisher's LSD (** $p < 0.01$, *** $p < 0.001$ compared to SDT and † $p < 0.05$ compared to 5-ALA). (E) Bar graphs show the decrease in tumor volume for 5 and 12 days after the treatment in PDT group. Statistical analyses were performed using two-tailed paired t-test (* $p < 0.05$). (F) Bar graphs show the decrease in tumor volume for 5 and 12 days after the treatment in SPDT group. There was no statistical significance when using two-tailed paired t-test. SDT, sonodynamic therapy; PDT, photodynamic therapy; SPDT, sono-photodynamic therapy.

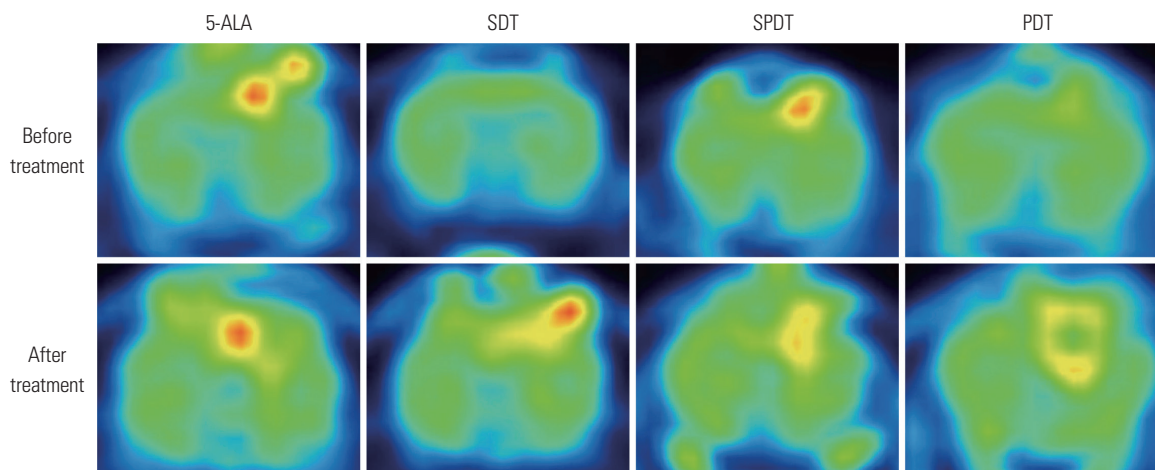


Fig. 4. Representative images of PET scan. After each treatment, the 5-ALA and SDT groups showed activated glucose uptake levels compared to the PDT and SPDT groups. SDT, sonodynamic therapy; PDT, photodynamic therapy; SPDT, sono-photodynamic therapy.

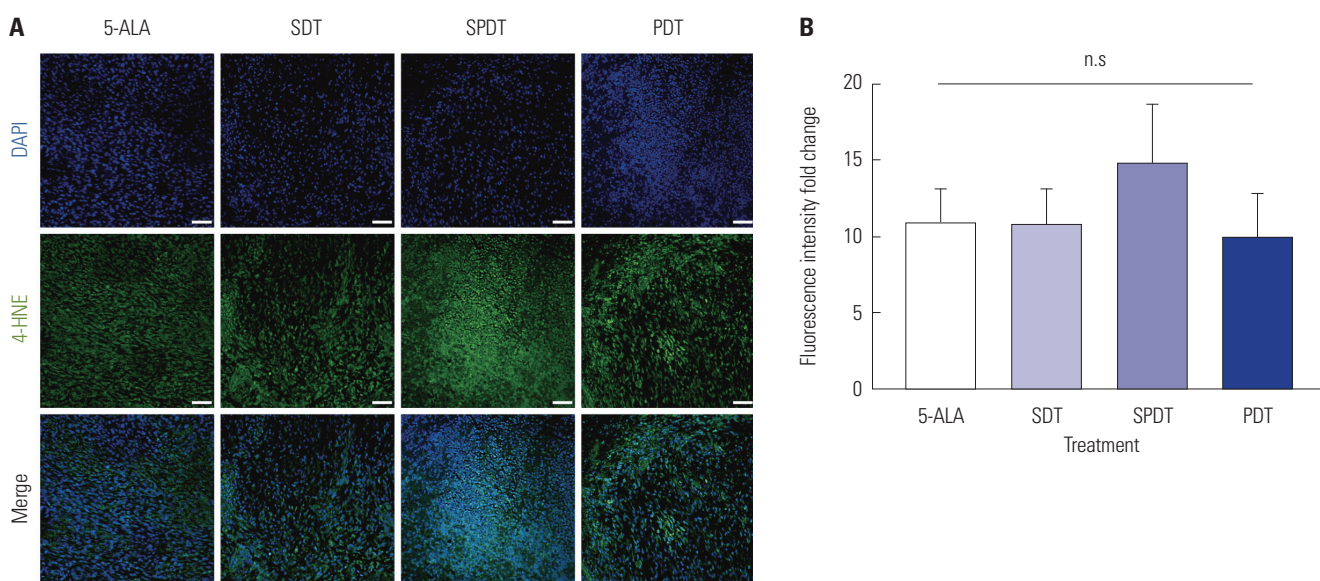


Fig. 5. Representative images of 4-HNE and analysis of IHC by comparing fluorescence intensity of each group. Data are presented as means \pm SEM. (A) Representative immunofluorescence images of 4-HNE (green) and DAPI (blue). Scale bar: 50 μ m. (B) Bar graphs show the intensity fold change of 4-HNE in the tumor relative to the 5-ALA group. Statistical analyses were performed using the Kruskal-Wallis test. There was no statistical significance between each group ($p=0.67$, $n=4$ for each group). SDT, sonodynamic therapy; PDT, photodynamic therapy; SPDT, sono-photodynamic therapy; IHC, immunohistochemistry; 4-HNE, 4-hydroxynonenal.

domly selected for MRI. Individual images were obtained using PMOD (Fig. 4). When PET images were compared after each treatment, the activated uptake of glucose level at the tumor site was observed in the 5-ALA and SDT groups, compared to the PDT and SPDT groups. The tumor site was divided by the contralateral standardized uptake values (SUVs) after conversion using PMOD (data not shown) for numerical comparison. There was no significant difference between groups due to the small number of subjects used in each group, but a slightly higher SUV value was found in the 5-ALA and SDT groups.

SPDT group showed a combined effect in generating ROS

A histological examination was performed to determine the

oxidative stress caused by ROS. After 3 days of treatment, animals were perfused for IHC analysis. Oxidative stress products, such as 4-HNE from lipid peroxidation and 8-OHdG from DNA oxidation, were measured via immunostaining. Representative images of 4-HNE in each group are shown in Fig. 5A, and the intensity expression levels showed no significance between the groups (5-ALA, 10.88 ± 2.17 ; SDT, 10.78 ± 2.41 ; SPDT, 14.82 ± 3.87 ; PDT, 9.91 ± 2.93 ; $p=0.67$) (Fig. 5B). However, in the case of 8-OHdG (Fig. 6A), the fluorescence intensity of the SPDT group showed a significant difference compared to that of each treatment group (5-ALA, 0.78 ± 0.34 , $p<0.001$; SDT, 1.70 ± 0.65 , $p=0.57$; PDT, 0.80 ± 0.35 , $p<0.001$ compared to SPDT, 5.61 ± 1.36) (Fig. 6B).

In addition, Caspase-3 levels were measured to analyze

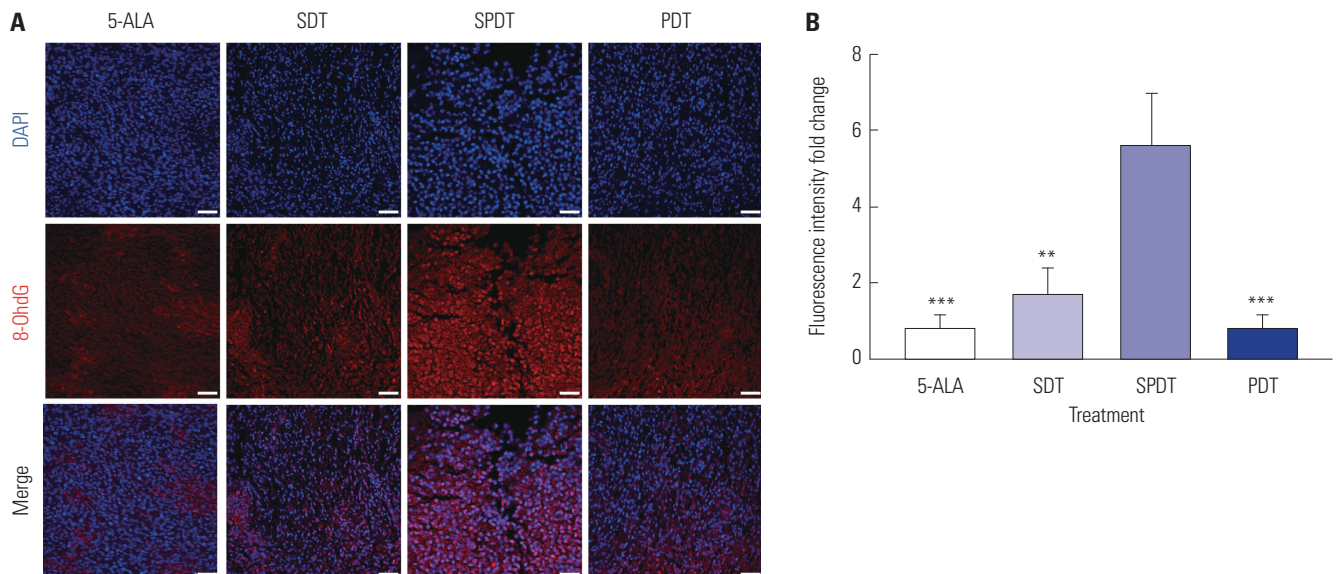


Fig. 6. Representative images 8-OHdG and analysis of IHC by comparing fluorescence intensity of each group. Data are presented as means \pm SEM. (A) Representative immunofluorescence images of 8-OHdG (red) and DAPI (blue). Scale bar: 50 μ m. (B) Bar graphs show the intensity fold change of 8-OHdG in the tumor relative to 5-ALA group. Statistical analyses were performed using the Kruskal-Wallis test (** p <0.01 and *** p <0.001 compared to SPDT, n =4 for each group). SDT, sonodynamic therapy; PDT, photodynamic therapy; SPDT, sono-photodynamic therapy; IHC, immunohistochemistry; 8-OHdG, 8-Hydroxy-2'-deoxyguanosine.

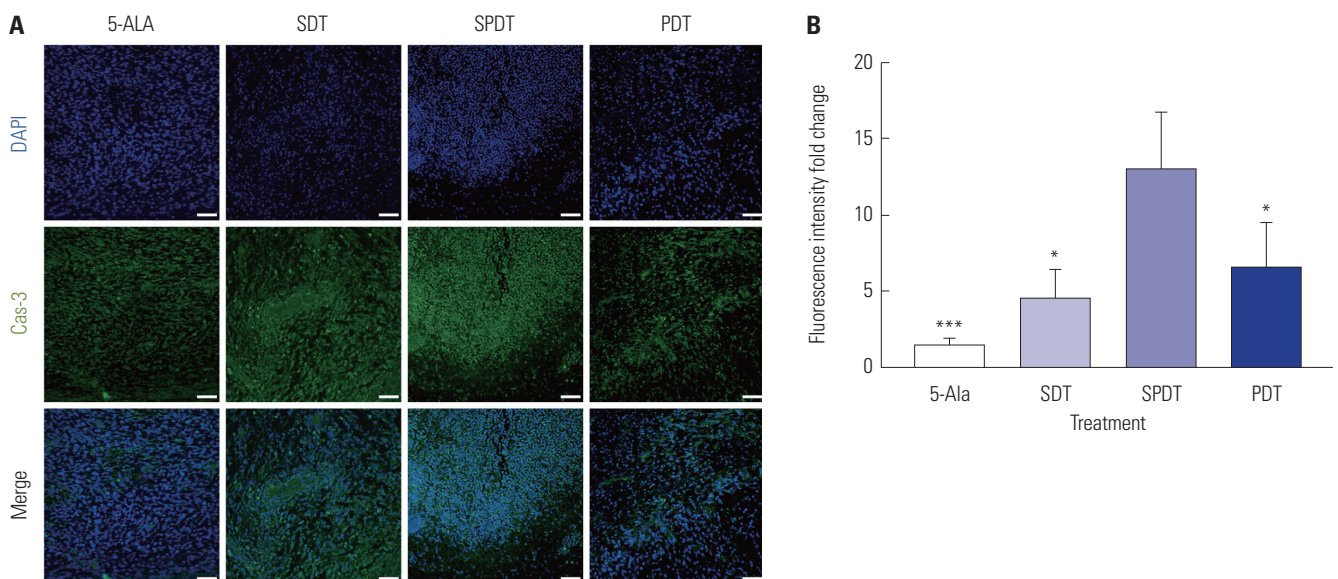


Fig. 7. Representative images of Cas-3 and analysis of IHC by comparing fluorescence intensity of each group. (A) Representative immunofluorescence images of cleaved Cas-3 (green) and DAPI (blue). Scale bar: 50 μ m. (B) Bar graphs show the intensity fold change of Cas-3 in the tumor relative to 5-ALA group. Data are presented as means \pm SEM. Statistical analyses were performed using the Kruskal-Wallis test (* p <0.05 and *** p <0.001 compared to SPDT, n =4 for each group). SDT, sonodynamic therapy; PDT, photodynamic therapy; SPDT, sono-photodynamic therapy; IHC, immunohistochemistry; Cas-3, Caspase-3.

apoptosis induction. Analysis of cleaved Caspase-3 was performed using the same method described above. Representative images of Caspase-3 in each group are shown in Fig. 7A. The SPDT group showed a significant difference compared to the 5-ALA and SDT groups (5-ALA, 1.32 ± 0.52 , p <0.001; SDT, 4.50 ± 1.82 , p =0.03; PDT, 6.52 ± 2.94 , p =0.04 compared to SPDT, 13.07 ± 3.7) (Fig. 7B). These findings indicate that the apoptosis process is more active in the SPDT group than in other groups.

DISCUSSION

Among the various treatments for tumors, PDT is of interest due to its non-invasive nature and tumor-selective benefits.⁷ However, the drawback of its transmission efficiency limits its usage in brain tumors.¹² Since ultrasound has better tissue transmittance than light, SDT draws attention as a way to treat the tumor and is being developed steadily.^{16,17} In addition,

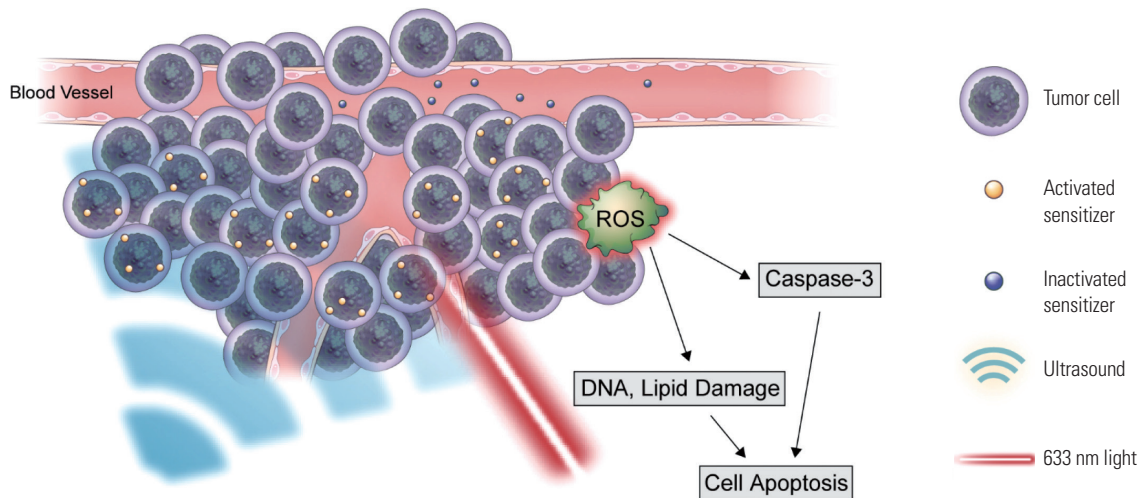


Fig. 8. Schematic of the expected operating principles of PDT and SDT. The sensitizer was activated by light or ultrasound energy to form reactive oxygen species (ROS). ROS affected tumor cells in various ways and induced apoptosis. SDT, sonodynamic therapy; PDT, photodynamic therapy.

SPDT, which combines PDT and SDT, is also of interest.²⁵ This study shows the effects and progress of three different treatment modalities in the C6 rat model; PDT, SDT, and SPDT (Fig. 8). The present study also demonstrated a decrease in tumor volume in the SPDT and PDT groups, which used light energy. However, SDT application had increased tumor volume after sonication, indicating that light energy was the leading cause of the tumor decrease, not ultrasound energy.

Tumor death induced by PDT is considered to be due to the following: 1) direct killing, 2) destruction of neovascularization, or 3) inflammatory and immune response.^{26,27} To confirm the therapeutic effect of PDT, Ki-67 expression and TUNEL assay, rather than factors corresponding to the apoptotic cascade, have often been used.²⁴ Since the core mechanism of these treatments is unclear, we analyzed the treatment efficacy by focusing on the expression level of ROS. By nature, ROS are highly reactive, making them difficult to image in biological tissues. Therefore, analyzing ROS relies on an indirect method of detecting its products by chemiluminescence or fluorescence, which are formed when they react with certain compounds.^{28,29} Therefore, this study conducted IHC analysis using 4-HNE, a second messenger in the ROS cascade, and 8-OHdG, which serves as a potential marker of DNA oxidation.^{30,31} Additionally, the degree of apoptosis induction by each treatment was determined using Caspase-3 as a marker.^{32,33} In consideration of the sufficient effect of treatment, the animals were sacrificed 3 days after the treatment.

As a result, the expression of oxidative stress increased only in the SPDT group, which may have had some synergistic effect of PDT and SDT. However, the PDT group showed no significant difference compared to the 5-ALA group (used as the control). Although IHC showed no significant findings, the MRI and PET findings of the PDT group showed that light successfully stimulated the sensitizer and led to tumor reduction. The difference in tumor volume between the groups was not signifi-

cant in MRI, 5 days after treatment. However, 12 days after treatment, not only did the tumor volume decrease significantly but also showed a significantly smaller size compared to SDT and 5-ALA injected groups. Also, reduced glucose uptake was observed in FDG-PET imaging. Therefore, IHC did not indicate a therapeutic effect due to the presence of ROS, but rather, the stabilized results of each factor over time. To date, there is no reference standard to confirm the treatment efficacy due to ROS in PDT studies.³⁴ Thus, further studies are needed to determine more accurate treatment effects.

Notably, the tumor volume in the SDT group was slightly higher than that in the control group at 12 days after treatment, though statistically insignificant. In addition, this group showed no difference in the IHC analysis, and the activated glucose uptake was similar to the control group even after the treatment, as shown in FDG-PET imaging. Although these findings were contrary to our hypothesis, it is considered that the characteristics of ultrasound energy lead to exacerbation of the tumor. FUS is widely used to modulate the microenvironment in the brain. One of the changes caused by ultrasound is the temporal up-regulation of vascular endothelial growth factor, which is a key factor of angiogenesis.³⁵ In a study of blood-brain barrier modulation using FUS with microbubble, it was reported that the factors associated with angiogenesis were also affected among the various factors after sonication.³⁶ Since the parameter used in this study did not differ significantly from those reported in the literature, it seemed that ultrasound also affected the vasculature of the GBM. Thus, it is presumed that the tumor volume was increased by activating tumor cells and their surroundings, rather than causing oxidative stress.

The sonication technique could also have impacted the outcomes in the SDT group. Ultrasound energy can be applied using diverse types of transducers or parameters in treating the tumor.^{37,38} Despite similar parameters used, as reported in the literature, the present study showed significantly different out-

comes.²⁴ Thus, our findings could imply that if ultrasound energy was not applied under precise control, it might promote the tumor microenvironment and even exacerbate it. Since the exact parameters to stimulate the sensitizer selective for the tumor by ultrasound have not been well-established, it may be premature to apply ultrasound to brain tumors; therefore, further studies are needed.³⁹

The SPDT group, which was given a combination of light and ultrasound energies simultaneously, showed comprehensive results. We initially hypothesized that SPDT would show increased efficiency due to the combination of the two energies, but our study showed different results. In MRI imaging, although the tumor volume was reduced, its size increased when compared to the PDT group, 12 days after treatment, which could be presumed to be due to the combined effects of successful stimulation of sensitizer by light and microenvironmental stimulation of ultrasound. However, compared to other groups, a significant upregulation of 8-ohdg and Caspase-3 was confirmed in IHC, and glucose absorption was also reduced in PET. Collectively, these findings show that stimulation using SPDT was effective, but did not last long and could not overcome the activation of the tumor by ultrasound. As a result, SPDT does not seem to be the most effective treatment, even though both energies were applied simultaneously.

This study has several limitations. First, the effectiveness of each treatment was analyzed from the perspective of ROS and apoptosis. Despite our effort, this is not a standard criterion, and the most effective treatment mechanism and time-point to maximize the efficacy are still unknown. Therefore, further studies on shorter periods, such as 12, 24, and 48 hours, may be required.³⁴ Second, since the parameter for FUS used was calculated under in vitro circumstances, the actual delivered power to the sensitizer used during SDT and SPDT is unknown. Thus, our findings should be interpreted with caution. To apply FUS precisely in SDT, further studies using additional equipment, such as thermal calculation, during sonication are required.⁴⁰

In conclusion, this study shows that PDT induces cytotoxicity and suppresses the growth of GBM. However, SDT did not suppress tumor but showed a tendency to exacerbate it. The findings of our study raise awareness of the ambivalent application of FUS for brain tumor therapy; thus, further study of optimal sonication parameters is required. SPDT, which is a combination of both energies, suppressed tumor growth and showed high therapeutic efficiency; however, these effects did not last long. Therefore, if the efficiency of the combined effect can be maintained and ultrasound energy can be accurately sonicated, this study might suggest that SPDT can be used to treat brain tumors efficiently.

ACKNOWLEDGEMENTS

This research was funded by the National Research Foundation of Korea (NRF), supported by the Ministry of Science, In-

formation and Communication Technology and Future Planning [NRF-2020RQA2C2008480], Samsung Research Funding & Incubation Center of Samsung Electronics under Project Number SRFC-IT2001-01, the Korea Medical Device Development Fund (KMDF_PR_20200901_0103), and “Dongwha” Faculty Research Assistance Program of Yonsei University College of Medicine (6-2020-0110). Medical Illustration & Design (MID), a part of the Medical Research Support Services of Yonsei University College of Medicine, provided excellent support with medical illustrations.

AUTHOR CONTRIBUTIONS

Conceptualization: Chanhong Kong, Jaewoo Shin, and Won Seok Chang. **Data curation:** Junwon Park, Chanhong Kong, and Jaewoo Shin. **Formal analysis:** Junwon Park, Chanhong Kong, Jaewoo Shin, Young Cheol Na, Jin Woo Chang, and Won Seok Chang. **Funding acquisition:** Won Seok Chang. **Investigation:** Junwon Park, Chanhong Kong, and Jaewoo Shin. **Methodology:** Junwon Park, Chanhong Kong, Jaewoo Shin, Ji Young Park, and Seung Hee Han. **Project administration:** Won Seok Chang. **Resources:** Seung Hyun Song and Won Seok Chang. **Software:** Chanhong Kong, Jaewoo Shin, and Seung Hee Han. **Supervision:** Seung Hyun Song and Won Seok Chang. **Validation:** Won Seok Chang. **Visualization:** Junwon Park, Chanhong Kong, and Won Seok Chang. **Writing—original draft:** Junwon Park. **Writing—review & editing:** Junwon Park, Chanhong Kong, Seung Hyun Song, and Won Seok Chang. **Approval of final manuscript:** all authors.

ORCID iDs

Junwon Park	https://orcid.org/0000-0003-0015-2744
Chanhong Kong	https://orcid.org/0000-0001-7987-7689
Jaewoo Shin	https://orcid.org/0000-0002-6335-1292
Ji Young Park	https://orcid.org/0000-0002-6912-9959
Young Cheol Na	https://orcid.org/0000-0001-5887-4788
Seung Hee Han	https://orcid.org/0000-0003-4900-3360
Jin Woo Chang	https://orcid.org/0000-0002-2717-0101
Seung Hyun Song	https://orcid.org/0000-0002-6181-4660
Won Seok Chang	https://orcid.org/0000-0003-3145-4016

REFERENCES

1. Davis ME. Glioblastoma: overview of disease and treatment. Clin J Oncol Nurs 2016;20(5 Suppl):S2-8.
2. Minniti G, Lanzetta G, Scaringi C, Caporello P, Salvati M, Arcella A, et al. Phase II study of short-course radiotherapy plus concomitant and adjuvant temozolomide in elderly patients with glioblastoma. Int J Radiat Oncol Biol Phys 2012;83:93-9.
3. Stupp R, Mason WP, van den Bent MJ, Weller M, Fisher B, Taphoorn MJ, et al. Radiotherapy plus concomitant and adjuvant temozolomide for glioblastoma. N Engl J Med 2005;352:987-96.
4. Perry JR, Bélanger K, Mason WP, Fulton D, Kavan P, Easaw J, et al. Phase II trial of continuous dose-intense temozolomide in recurrent malignant glioma: RESCUE study. J Clin Oncol 2010;28:2051-7.
5. Wilson TA, Karajannis MA, Harter DH. Glioblastoma multiforme: state of the art and future therapeutics. Surg Neurol Int 2014;5:64.
6. Díez Valle R, Hadjipanayis CG, Stummer W. Established and emerging uses of 5-ALA in the brain: an overview. J Neurooncol 2019;141:487-94.

7. Kessel D. Photodynamic therapy: a brief history. *J Clin Med* 2019; 8:1581.
8. Kelly JF, Snell ME, Berenbaum MC. Photodynamic destruction of human bladder carcinoma. *Br J Cancer* 1975;31:237-44.
9. Kwiatkowski S, Knap B, Przysupski D, Saczko J, Kędzierska E, Knap-Czop K, et al. Photodynamic therapy-mechanisms, photosensitizers and combinations. *Biomed Pharmacother* 2018;106: 1098-107.
10. Goryaynov SA, Widhalm G, Goldberg MF, Chelushkin D, Spallone A, Chernyshov KA, et al. The role of 5-ALA in low-grade gliomas and the influence of antiepileptic drugs on intraoperative fluorescence. *Front Oncol* 2019;9:423.
11. Mahmoudi K, Garvey KL, Bouras A, Cramer G, Stepp H, Jesu Raj JG, et al. 5-aminolevulinic acid photodynamic therapy for the treatment of high-grade gliomas. *J Neurooncol* 2019;141:595-607.
12. Akimoto J, Fukami S, Suda T, Ichikawa M, Haraoka R, Kohno M, et al. First autopsy analysis of the efficacy of intra-operative additional photodynamic therapy for patients with glioblastoma. *Brain Tumor Pathol* 2019;36:144-51.
13. Hu T, Wang Z, Shen W, Liang R, Yan D, Wei M. Recent advances in innovative strategies for enhanced cancer photodynamic therapy. *Theranostics* 2021;11:3278-300.
14. Kim A, Zhou J, Samaddar S, Song SH, Elzey BD, Thompson DH, et al. An implantable ultrasonically-powered micro-light-source (ulight) for photodynamic therapy. *Sci Rep* 2019;9:1395.
15. Etcheverry ME, Pasquale MA, Garavaglia M. Photodynamic therapy of HeLa cell cultures by using LED or laser sources. *J Photochem Photobiol B* 2016;160:271-7.
16. Shibaguchi H, Tsuru H, Kuroki M, Kuroki M. Sonodynamic cancer therapy: a non-invasive and repeatable approach using low-intensity ultrasound with a sonosensitizer. *Anticancer Res* 2011; 31:2425-9.
17. McHale AP, Callan JF, Nomikou N, Fowley C, Callan B. Sonodynamic therapy: concept, mechanism and application to cancer treatment. *Adv Exp Med Biol* 2016;880:429-50.
18. Rengeng L, Qianyu Z, Yuehong L, Zhongzhong P, Libo L. Sonodynamic therapy, a treatment developing from photodynamic therapy. *Photodiagnosis Photodyn Ther* 2017;19:159-66.
19. O'Brien WD Jr. Ultrasound-biophysics mechanisms. *Prog Biophys Mol Biol* 2007;93:212-55.
20. Kim J, Shin J, Kong C, Lee SH, Chang WS, Han SH. The synergistic effect of focused ultrasound and biophotonics to overcome the barrier of light transmittance in biological tissue. *Photodiagnosis Photodyn Ther* 2021;33:102173.
21. Kim H, Chang JH. Increased light penetration due to ultrasound-induced air bubbles in optical scattering media. *Sci Rep* 2017;7: 16105.
22. Li Q, Liu Q, Wang P, Feng X, Wang H, Wang X. The effects of Ce6-mediated sono-photodynamic therapy on cell migration, apoptosis and autophagy in mouse mammary 4T1 cell line. *Ultrasonics* 2014;54:981-9.
23. Zhu JX, Zhu WT, Hu JH, Yang W, Liu P, Liu QH, et al. Curcumin-loaded poly(L-lactide-co-glycolide) microbubble-mediated sono-photodynamic therapy in liver cancer cells. *Ultrasound Med Biol* 2020;46:2030-43.
24. Wu SK, Santos MA, Marcus SL, Hynynen K. MR-guided focused ultrasound facilitates sonodynamic therapy with 5-aminolevulinic acid in a rat glioma model. *Sci Rep* 2019;9:10465.
25. Tserkovsky DA, Alexandrova EN, Chalau VN, Istomin YP. Effects of combined sonodynamic and photodynamic therapies with photolon on a glioma C6 tumor model. *Exp Oncol* 2012;34:332-5.
26. Sánchez V, Garcia MR, Requena MB, Romano RA, de Boni L, Guimarães FEG, et al. Theoretical and experimental analysis of protoporphyrin IX photodegradation using multi-wavelength light sources. *Photochem Photobiol* 2020;96:1208-14.
27. Anand S, Chan TA, Hasan T, Maytin EV. Current prospects for treatment of solid tumors via photodynamic, photothermal, or ionizing radiation therapies combined with immune checkpoint inhibition (a review). *Pharmaceuticals (Basel)* 2021;14:447.
28. Pryor WA, Godber SS. Noninvasive measures of oxidative stress status in humans. *Free Radic Biol Med* 1991;10:177-84.
29. Freeman BA, Crapo JD. Biology of disease: free radicals and tissue injury. *Lab Invest* 1982;47:412-26.
30. Jaganjac M, Milkovic L, Gegotek A, Cindric M, Zarkovic K, Skrzydlewska E, et al. The relevance of pathophysiological alterations in redox signaling of 4-hydroxynonenal for pharmacological therapies of major stress-associated diseases. *Free Radic Biol Med* 2020;157:128-53.
31. Shahmoradi Ghahe S, Kosicki K, Wojewódzka M, Majchrzak BA, Fogtman A, Iwanicka-Nowicka R, et al. Increased DNA repair capacity augments resistance of glioblastoma cells to photodynamic therapy. *DNA Repair (Amst)* 2021;104:103136.
32. Arslan H, Altun S, Özdemir S. Acute toxication of deltamethrin results in activation of iNOS, 8-OHdG and up-regulation of caspase 3, iNOS gene expression in common carp (*Cyprinus carpio* L.). *Aquat Toxicol* 2017;187:90-9.
33. Namura S, Zhu J, Fink K, Endres M, Srinivasan A, Tomaselli KJ, et al. Activation and cleavage of caspase-3 in apoptosis induced by experimental cerebral ischemia. *J Neurosci* 1998;18:3659-68.
34. Cauchon N, Turcotte E, Lecomte R, Hasséssian HM, Lier JE. Predicting efficacy of photodynamic therapy by real-time FDG-PET in a mouse tumour model. *Photochem Photobiol Sci* 2012;11:364-70.
35. McMahon D, Mah E, Hynynen K. Angiogenic response of rat hippocampal vasculature to focused ultrasound-mediated increases in blood-brain barrier permeability. *Sci Rep* 2018;8:12178.
36. Kovacs ZI, Kim S, Jikaria N, Qureshi F, Milo B, Lewis BK, et al. Disrupting the blood-brain barrier by focused ultrasound induces sterile inflammation. *Proc Natl Acad Sci U S A* 2017;114:E75-84.
37. Roberts JW, Powlovich L, Sheybani N, LeBlang S. Focused ultrasound for the treatment of glioblastoma. *J Neurooncol* 2022;157: 237-47.
38. Joiner JB, Pylayeva-Gupta Y, Dayton PA. Focused ultrasound for immunomodulation of the tumor microenvironment. *J Immunol* 2020;205:2327-41.
39. Ho YJ, Li JP, Fan CH, Liu HL, Yeh CK. Ultrasound in tumor immunotherapy: current status and future developments. *J Control Release* 2020;323:12-23.
40. van Rhoon GC, Samaras T, Yarmolenko PS, Dewhurst MW, Neufeld E, Kuster N. CEM43°C thermal dose thresholds: a potential guide for magnetic resonance radiofrequency exposure levels? *Eur Radiol* 2013;23:2215-27.